Nucleobase-functionalized grapheme nanoribbons for accurate high-speed DNA sequencing

Paulechka, Eugene; Wassenaar, Tsjerk; Kroenlein, Kenneth; Kazakov, Andrei; Smolyanitsky, Alex

Published in:
Nanoscale

DOI:
10.1039/C5NR07061A

Publication date:
2016

Nanoscale

COMMUNICATION

View Article Online
View Journal | View Issue

Cite this: *Nanoscale*, 2016, **8**, 1861

Received 12th October 2015,
Accepted 22nd December 2015

DOI: 10.1039/c5nr07061a

www.rsc.org/nanoscale

Nucleobase-functionalized graphene nanoribbons for accurate high-speed DNA sequencing†

Eugene Paulechka,[a] Tsjerk A. Wassenaar,[b,c] Kenneth Kroenlein,[a] Andrei Kazakov[a] and Alex Smolyanitsky*[a]

We propose a water-immersed nucleobase-functionalized suspended graphene nanoribbon as an intrinsically selective device for nucleotide detection. The proposed sensing method combines Watson–Crick selective base pairing with graphene's capacity for converting anisotropic lattice strain to changes in an electrical current at the nanoscale. Using detailed atomistic molecular dynamics (MD) simulations, we study sensor operation at ambient conditions. We combine simulated data with theoretical arguments to estimate the levels of measurable electrical signal variation in response to strains and determine that the proposed sensing mechanism shows significant promise for realistic DNA sensing devices without the need for advanced data processing, or highly restrictive operational conditions.

Fast, reliable, and cost-effective DNA sequencing continues to be an important open problem, as the vast majority of sequencing needs currently remains to be satisfied by the use of the Sanger method.[1] Despite the numerous advances made in automation and data analysis as part of the Human Genome Project,[2,3] the throughput rate and cost still significantly limit routine production of genomic data using the currently available technology.

Various alternative approaches have been proposed, ranging from employing ionic current blockage by DNA nucleotides in aqueous nanopores[4,5] to the use of chemically selective tunneling current probes.[6] Discovery of atomically thin carbon allotropes and their exceptional electronic, mechanical, and chemical properties has reinvigorated the search for nanoscale system based DNA sequencing methods in the past decade. Consequently, numerous graphene-based approaches have been proposed, mostly centered on the use of graphene as the ultimately thin membrane impermeable to water-dissolved ions[7–10] and nanoscale graphene-based field-effect transistor devices with nucleotide-specific electronic response.[11–15] In all proposed methods, robust single-measurement nucleobase selectivity in realistic measurement conditions naturally remains a fundamental challenge.[16,17] with single nucleotide count errors of up to 90%,[18] depending on the approach. In addition, device noise in ambient conditions remains one of the most serious problems in developing a robust graphene-based sensing methodology.[12]

Here, we report on utilizing graphene's electronic properties, effectively combined with the Watson–Crick base-pairing, as a possible method of high-speed DNA sequencing at ambient conditions in aqueous environment. The key feature of the proposed method is a graphene nanoribbon (GNR) with a nanoscale opening, the interior of which is chemically functionalized with selected nucleobases. As sketched in Fig. 1(a), a single-strand DNA (ssDNA) molecule is inserted into the functionalized pore and translocated at a prescribed rate perpendicularly to the GNR. When a base complementary to the GNR's functional group traverses the pore during translocation, selective hydrogen bond formation is expected to occur, as shown in Fig. 1(b), provided there is sufficient dwell time set by the prescribed translocation rate. As a result of local DNA–GNR binding, the GNR is expected to be temporarily pulled upon and deflected in the out-of-plane direction, followed by a slip when the critical force required for breaking the hydrogen bonds is reached. Although direct microscopy-based methods of detecting such deflections are possible, here we focus on the possibility of utilizing the effect of deflection-induced strain on the electronic properties of the GNR, and thus detecting a temporary change in the electrical current (from the electrical bias, as sketched in Fig. 1(a)), as discussed later. Therefore, temporary changes in the electrical current can serve as electrically measurable nucleobase detection events. Given that C/G-functionalized GNR is a G/C-selective, while an A/T-functionalized GNR is T/A-selective, vertically stacking a total of four independently biased and

[a]*Applied Chemicals and Materials Division, National Institute of Standards and Technology, Boulder, CO 80301, USA. E-mail: alex.smolyanitsky@nist.gov*
[b]*Department of Biology, Friedrich-Alexander University of Erlangen-Nürnberg, 91058 Erlangen, Germany*
[c]*Groningen Biomolecular Sciences and Biotechnology Institute and Zernike Institute for Advanced Materials, University of Groningen, 9747 AG Groningen, The Netherlands*

†Electronic supplementary information (ESI) available. See DOI: 10.1039/c5nr07061a

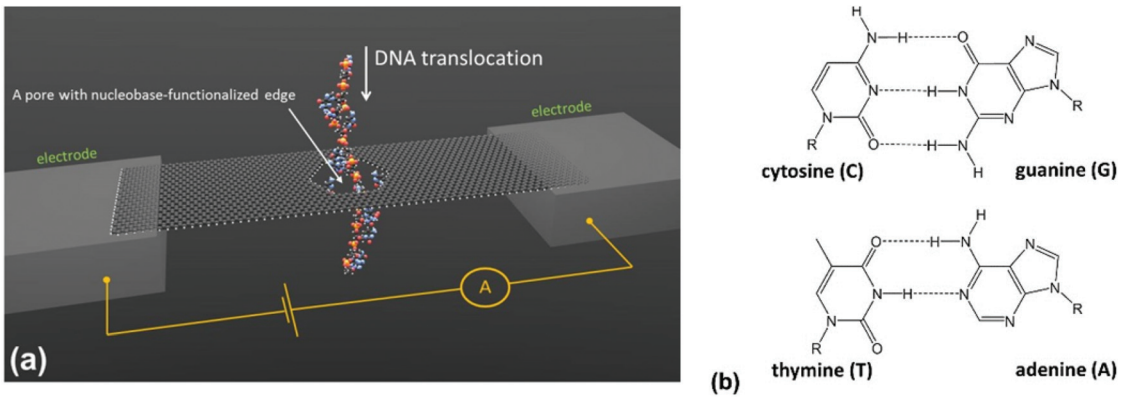

Fig. 1 A three-dimensional sketch of the proposed nucleobase sensor (a) and the Watson–Crick base-pairing principle (b). The dotted lines in (b) represent the hydrogen bonds formed between the nucleobases.

appropriately functionalized GNRs would result in an integrated sequence detector.

Here, we present the results of carefully designed atomistic molecular dynamics (MD) simulations of the continuous ssDNA translocation through a C-functionalized GNR in an aqueous environment. Our simulations are aimed at assessing the selectivity of detecting G nucleobases in terms of the effective GNR deflection at room temperature.

Shown in Fig. 2(a) is the central portion of the sensor, which consists of a L_x = 4.5 nm × L_y = 15.5 nm GNR with a ~2.5 nm – wide nanopore, whose interior is functionalized with three cytosine molecules. The GNR is position-restrained at the ends, mimicking suspension between solid electrodes. The carbon atom at position six in the cytosine molecule was covalently attached to an edge carbon[19] in the pore of the functionalized GNR (FGNR), as seen in the magnification in Fig. 2(a). Such an attachment point keeps the hydrogen-bonding groups facing the interior of the nanopore, and thus available for interaction with the side-chains of the nucleotides subject to sensing. The atomic-level geometry of the cytosine-functionalized region, including the near-90° orientation (consistent with previous calculations[20]) of the cytosine moiety relative to the graphene plane, was obtained from a DFT energy optimization of an anthracene molecule, functionalized by the cytosine moiety at position nine. As shown in Fig. 2(b), six-residue ssDNA samples (sequences defined further) periodic in the Z-direction was inserted into the nanopore, as shown in Fig. 2(c). All DNA backbones were pre-stretched in the Z-direction by a force of ~0.1 nN in order to promote strand linearity. In addition, weak positional restraint in the XY-plane was applied to the ssDNA backbone, so it on average remained close to the center of the nanopore, essentially mimicking a precision aperture. All MD simulations of the DNA translocation process were performed at ambient conditions (T = 300 K, p = 0.1 MPa). The DFT optimization of the GNR functional region was performed with the use of Gaussian 09[21] at the B3LYP/6-31+G(d) theory level.[22,23] All partial atomic charges in the functional group were calculated according to the CHELPG scheme[24] at the HF/6-31+G(d) theory level for the optimized geometry. The MD models of the ssDNA and the FGNR were based on the OPLS-AA force field.[25,26] The intramolecular interaction parameters for graphene were obtained from the optimized bond-order potential for carbon,[27] as described elsewhere.[28] As shown in Fig. 2(c), the entire system was immersed in a rectangular box filled with water described by the TIP4P model.[29,30] Prior to the production MD runs, the systems were carefully pre-relaxed in NPT simulations at T = 300 K and p = 0.1 MPa, while the production simulations of DNA translocation were performed in an NVT ensemble at T = 300 K, using GROMACS v. 5.0.5 software.[31,32]

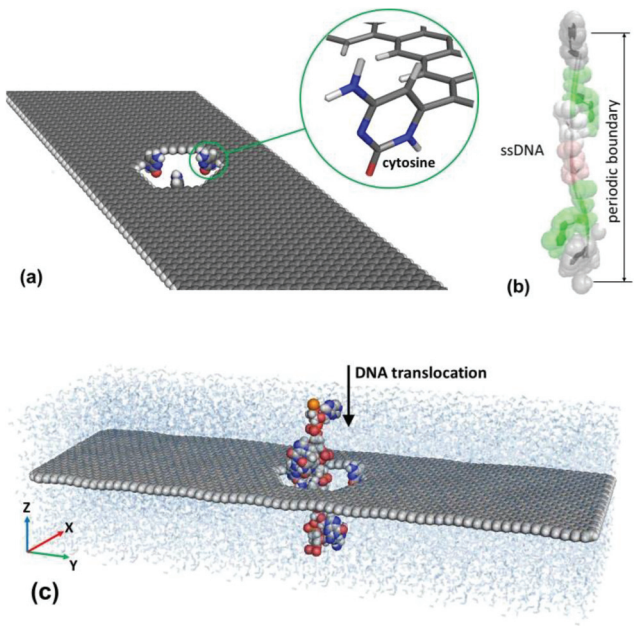

Fig. 2 An atomistic model of a graphene nanoribbon with cytosine-functionalized nanopore (a), periodic ssDNA (b), and the complete simulated assembly immersed in water (c).

The results obtained in a simulated ssDNA translocation aimed at sensing the G residues by a C-functionalized GNR are

discussed next. We used two arbitrarily selected six-residue periodic sequences of ***GAAGCT*** (SEQ1) and *TC**G**AAC* (SEQ2) translocated in the negative-*Z* direction at a constant rate of 5 cm s^{-1}, as dictated by the MD time limitations for a system of this size. The FGNR in all cases was pre-stretched at the ends (along the *Y*-axis) by 0.5% to enable a rapid return to post-deflection unperturbed state and to somewhat suppress the thermal fluctuations. The total simulated time was 300 ns, during which the sequences translocated through the pore were repeated approximately 3.3 times. In the case of SEQ1, this effectively corresponds to ***G**AAGCT/**G**AAGCT/**G**AAGCT/**G**A*, and thus seven passes of the G residue are expected. For SEQ2, the corresponding sequence is *TC**G**AAC/TC**G**AAC/TC**G**AAC/TC* with three expected passes of G. Note that the nucleobase inside the pore at the start of a simulation (underlined) can vary, because the pre-translocation MD relaxation steps for the various systems discussed here allowed for spurious translocation of the sample ssDNA. As seen further, the variation in the starting residue does not affect the clarity of our observations, as we effectively track the passage of the G-bases. Shown in Fig. 3(a) we present the results of SEQ1 translocation in the form of the out-of-plane deflection of the GNR as a function of

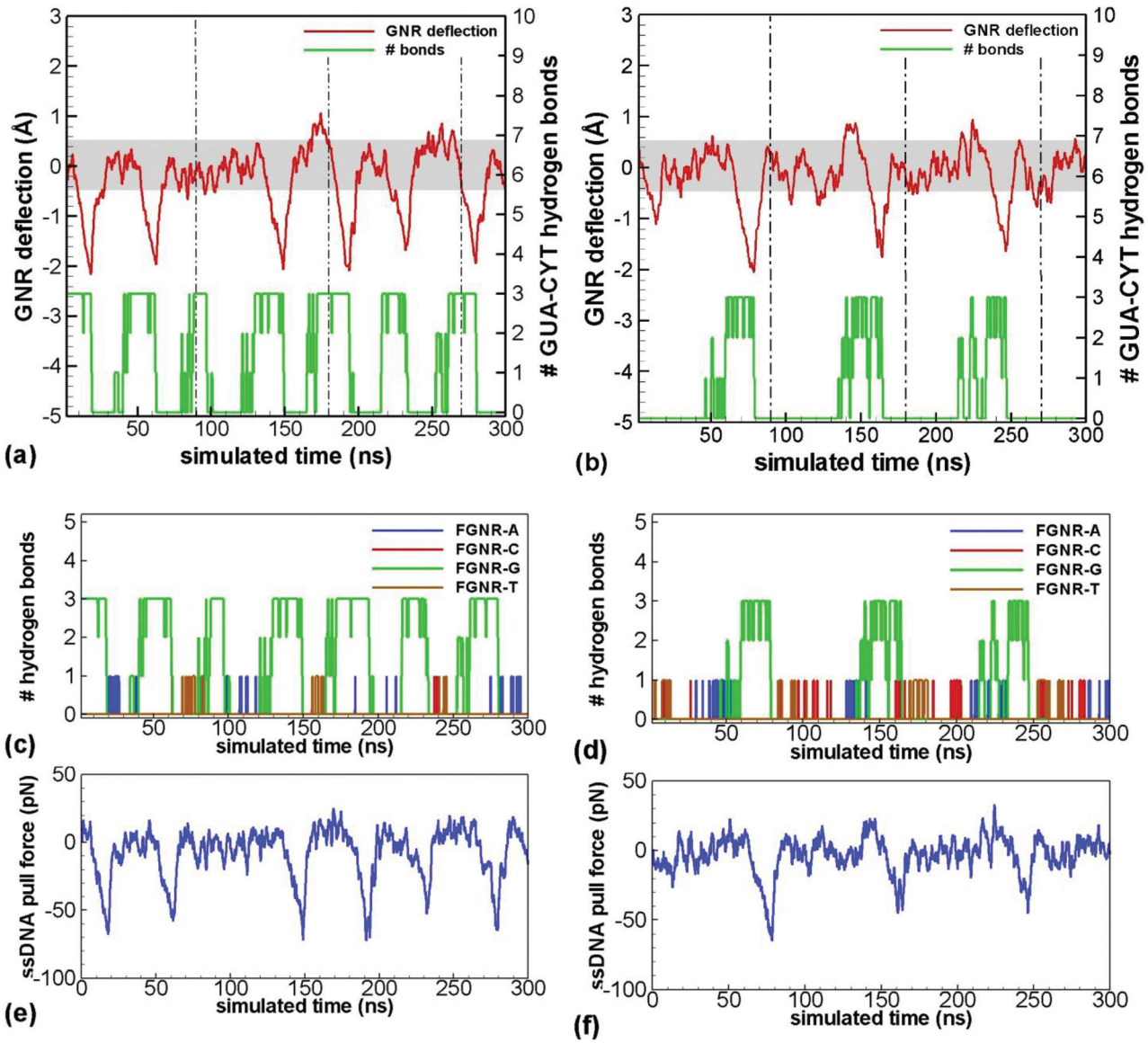

Fig. 3 FGNR deflection and the number of G–C hydrogen bonds as functions of simulated time for ssDNA sequence SEQ1 (periodic ***G**AAGCT*) (a) and sequence SEQ2 (periodic *TC**G**AAC*) (b); all hydrogen bonds between the FGNR and the ssDNA sequence SEQ1 (c) and SEQ2 (d); ssDNA pulling force during translocation of SEQ1 (e) and SEQ2 (f). The ssDNA translocation speed in these simulations was 5 cm s^{-1}, approximately corresponding to 66 million of nucleobases per second. The grey strips in (a) and (b) represent a background noise measure: the strip half-width is $\sqrt{2}$ × deflection RMSD from the regions of non-G translocation in (b). A low-pass filter with an effective bandwidth of 500 MHz was applied to the raw deflection and pulling force data.

simulated time, shown alongside the number of hydrogen bonds formed between the functional groups and the G residues in the tested ssDNA. The latter measure enables clear tracking of the residue of interest, as it passes through the pore. As expected, a total of seven binding events occur between the functional groups at the pore interior and the residues of interest. A total of three hydrogen bonds are created in each case, as shown in Fig. 3(a), consistent with the schematic representation in Fig. 1(b). Remarkably, in six out of the seven G-passage events, the bond formation is accompanied by a clear GNR out-of-plane deflection of the average ~2 Å magnitude, followed in each case by a sharp slip when the critical force required for breaking the G–C hydrogen bonds was reached. The clearly missed event is located at $t \approx 100$ ns. Interestingly, as observed in Fig. 3(e), the critical pulling force in the range 50–80 pN, consistent with the experimentally measured 54.0–61.4 pN.[33,34] Note that for a sensor aimed at detecting the A/T bases (with a T/A-functionalized GNR), the corresponding critical force would be ~2/3 of the average C–G value, reducing the corresponding deflection magnitude accordingly (see ESI†). In Fig. 3(b, d and f), the same data is presented for SEQ2. Similarly, the passage of the G-nucleobase is accompanied by a temporary GNR deflection in all of the three cases. It is noteworthy that no post-processing of the deflection data was performed beyond basic low-pass filtering with a bandwidth of 500 MHz, as stated in the figure legend. Such filtering allowed effective removal of thermal noise, as well as clear resolution of the deflection events, which, from the presented data, took ~15 ns on average, thus corresponding to an effective frequency of ~66 MHz.

The intended ssDNA–FGNR chemical coupling can be seen in Fig. 4, where a representative deflected state of the FGNR immediately prior to pull-off is shown. The interacting groups are properly oriented and the hydrogen bonds are formed between the functional group at the nanopore edge and the passing G-base. Importantly, no false-positives occurred during simulated translocation, likely due to no significant hydrogen bond formation between the FGNR and the non-guanine nucleobases in the test sample. This cause for the demonstrated level of selectivity is supported by the data in Fig. 3(c and d), where all "spurious" hydrogen bonds are tracked throughout the simulated time alongside the intended (FGNR-G) bonds.

The translocation rate is expected to greatly affect the device performance in terms of the bond formation and the overall system relaxation, resulting in effects on the noise, and nucleobase selectivity. Therefore, we performed translocation tests of SEQ1 at a significantly higher rate of 25 cm s^{-1}, corresponding approximately to 330 million nucleobases per second, simulated for 60 ns. The resulting FGNR deflection and the number of C–G hydrogen bonds as functions of time are shown in Fig. 5. Although C–G bonds continue to form between the FGNR and the passing ssDNA, and the average deflection magnitude is higher (likely due to lack of system relaxation), the detection quality here is noticeably worse. In particular, we observe a noisy resolution of the G passage at $t \approx 10$ ns and a missed event at $t \approx 35$ ns.

Although one cannot claim true statistical significance from the results of atomistic simulations describing translocation of only ten sequencing events, our combined data in Fig. 3(a and b) suggest an overall single-sensor detection error probability in the vicinity of 1/10 for the 5 cm s^{-1} translocation rate. Given that no false positives were observed, one roughly estimates that a total of four independent measurements would be required to achieve a 99.99% fidelity at the translocation rate of 5 cm s^{-1}. In addition, given that an experimental setup would likely use even lower translocation speeds, the overall single-measurement error rate may be further improved.

As mentioned earlier, the nucleotide passage can be in principle detected in an atomic force microscopy-like setup by

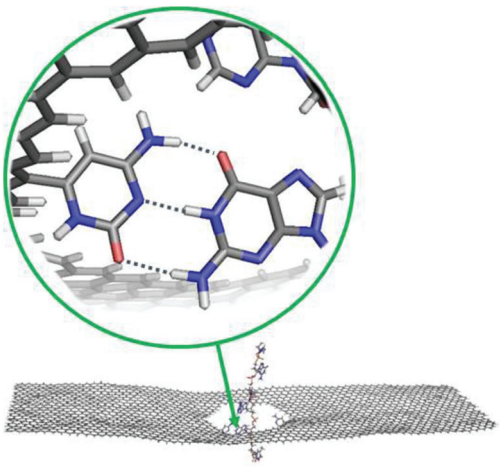

Fig. 4 A representative deflected state of the FGNR prior to G–C detachment.

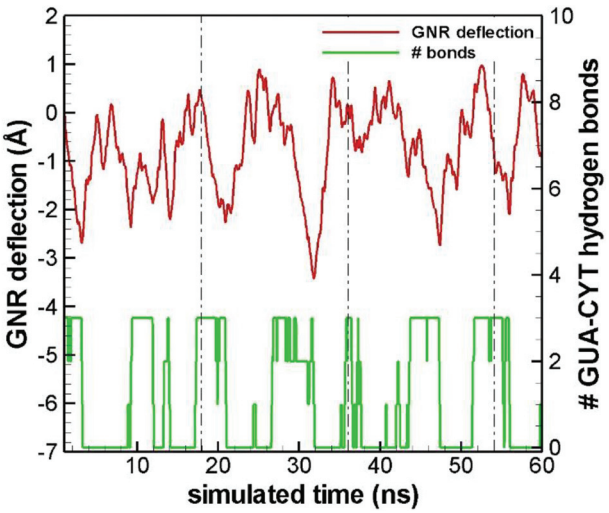

Fig. 5 FGNR deflection and the number of G–C hydrogen bonds as functions of simulated time during ssDNA (SEQ1) translocation at the rate of 25 cm s^{-1}. A low-pass filter with an effective bandwidth of 2.5 GHz was applied to the raw deflection data.

tracking the deflections directly, or by monitoring the FGNR–DNA interaction forces (shown in Fig. 3(e and f)). However, direct electronic detection of the nanoscale deflection is a highly attractive option. Although a truly accurate estimate of the electrical current changes in a transversely deflected FGNR would depend on the GNR quality, edge geometry (zigzag or armchair), and dimensions, a theoretical discussion at the order-of-magnitude level is possible. Electronic deflectometry based on the effect of strain on the electronic band structure of carbon nanotubes and graphene has been studied in detail experimentally[35] and theoretically.[36,37] Assuming negligible contact resistance and positing that thermally activated carriers in the conduction band dominate at T = 300 K, the Landauer formalism yields a relative change in electrical resistance of a GNR of the order $\frac{\Delta R}{R} \approx \frac{\Delta E_{gap}}{kT}$,[35] where R is the electrical resistance, ΔE_{gap} is the energy bandgap modulation at the Dirac point due to the deflection-induced uniaxial strain (regardless of the existing bandgap in an undeflected state due to GNR edge type, width, *etc.*) and k is the Boltzmann constant. A tight-binding estimate for the effect of uniaxial strain ε is $\Delta E_{gap} \propto 3t_0\varepsilon$ ($t_0 \approx 2.7$ eV) is the nearest-neighbor electron hopping energy for graphene).[38] For a GNR of length L deflected by $h \ll L$, $\varepsilon \approx 2(h/L)^2$, and thus for the FGNR dimensions and h = 2 Å in this work, we estimate ε = 0.033%, yielding a positive $\frac{\Delta R}{R} = 10.4\%$ due to the largeness of the (t_0/kT) ratio, and thus resulting in an appreciable average current decrease.

If, depending on the GNR, coherent transport dominates the conductive process, the effect of strain on an ungated GNR would be negligible.[36] Thus, an effective use of a gate electrode was suggested,[36] which enables modification of the carrier transmission probability and results in an effective relative change in conductance of the order (h^2/La_0), where a_0 = 1.42 Å is the C–C bond length in graphene. The latter estimate yields a relative change of ≈2% for the deflected GNR considered here. This net change is not particularly high, but is experimentally detectable and is higher in larger GNRs. Recall that this work considers a short and narrow GNR (dictated by the computational limitations of MD). In an experimental setup, a considerably wider and longer GNR would be used. The deflection-to-length ratio is $\frac{h}{L} \sim (F_c/w)^{1/3}$, where w is the GNR width and F_c is the critical C–G shearing force (see ESI†), and thus the amount of deflection could be increased in a longer and wider GNR with a somewhat higher aspect ratio. For instance, a 10 nm × 60 nm GNR would be deflected (at F_c = const) by ≈6.4 Å, thus resulting in a relative average current shift by ≈4.8%. In a GNR with the original dimensions and without lateral pre-strain, the two detection mechanisms discussed above yield a relative change in resistance of 71% and 12%, respectively. See sections S1 and S2 of ESI† for details, as well as further discussion on the GNR size effects.

Because the locally suspended FGNR is part of an aqueous system, subject to interaction with water and the nanopore-confined DNA molecule, the effect of dynamic ripples on the GNR can introduce an additional source of charge carrier scattering and noise, compared to "conventional" solid-state devices. As estimated in the ESI,† the ripple scattering strength is decreased as a result of deflection-induced strain. Therefore, if ripple scattering is expected to significantly contribute to the overall resistance in a given GNR, the observed effect may become a contributing mechanism, suggesting an additional design consideration in terms of the GNR dimensions, edge type, and doping parameters. The rippling process is intrinsically dynamic in suspended atomically thin membranes, causing significant rippling mean-square variation in the time domain (see Fig. S1 of the ESI†). This suggests a temporal modulation of the local electron hopping parameters, and thus an additional source of rippling-induced noise. However, because the timescale of the ripple dynamics is fundamentally linked to the flexural wave propagation velocity in graphene of the order of kilometers per second,[39] the dynamic modulation of current occurs at the picosecond timescale,[40] unless the effective GNR dimensions reach tens of microns. Thus, given that the timescale of the deflection-induced signal is of the order of tens of nanoseconds for the translocation rate of 5 cm s^{-1} (~15 ns per base), and expected to be further lowered in an experiment (currently 1–3 μs per base[41]), one can argue that basic low-pass signal filtering should be sufficient to eliminate the high-frequency current noise arising from the FGNR fluctuations.

As a result of its hydrophobicity, graphene is likely to adsorb a DNA strand in the case of lack of positional precision during insertion and translocation in an experiment, suggesting a significant effect on the overall measurement accuracy. A possible way to alleviate this potential problem is by locally tailoring graphene hydrophobicity in the vicinity of the nanopore *via* non-covalent coating,[42] expected to also affect the GNR flexibility and thus the amount of strain-inducing deflection. In addition, the concept outlined here is extendable toward any non-hydrophobic atomically thin membranes with sufficient sensitivity of the electronic properties to anisotropic strain, *e.g.* molybdenum disulfide.[43]

Conclusions

We have proposed a cytosine-functionalized graphene nanoribbon deflectometer in aqueous environment at ambient conditions for fast and accurate sensing of nucleotides during continuous translocation of intact ssDNA. The proposed sensing mechanism combines Watson–Crick complementary base pairing with the sensitivity of graphene's electronic properties to anisotropic strain, as well as the deflection-induced field effects described in the literature. Our simulations demonstrate single-sensor guanine detection accuracy in the vicinity of 90% with no false-positives at the translocation rate of ~66 million nucleobases per second. We estimate that the strain effects on the electrical conductance of graphene nanoribbons at ambient conditions are measurable, requiring only

basic low-pass signal filtering, and thus rapid sequencing may be effectively reduced to an electrical current measurement in the milliampere range (as dictated by a typical electrical resistance of a GNR[13]) without the need for microscopy-based methods. With the exception of the proposed nucleobase functionalization, all of the individual components of the proposed sensing method have been previously implemented experimentally. The proposed sensing methodology may therefore hold significant promise for realistic DNA sequencing devices without the need for advanced data processing, or highly restrictive operational conditions, especially given its extendibility toward other strain-sensitive membranes.

Authors' contributions

A.S. conceived the sensor concept and supervised the project. E.P. developed and detailed GNR functionalization, and devised DFT simulations. A.S. and E.P. designed MD simulations and analyzed the data. T.A.W. built the DNA model and automated system design. T.A.W. and A.S. performed MD simulations. K.K. devised and implemented data analysis software. A.K. performed DFT simulations and contributed to the data analysis software. All authors discussed the results, composed the manuscript, and contributed to revisions.

Acknowledgements

The authors are grateful to A. Isacsson and D.K. Ferry for illuminating discussions. T.A.W. acknowledges support by S.J. Marrink and the generous computational support by the Donald Smit Center at the University of Groningen. A.S. acknowledges the computational support by the NIST Center for Theoretical and Computational Materials Science and personally thanks A.C.E. Reid. We also thank L. Rast for providing outstanding assistance with graphics.

This work is a contribution of the National Institute of Standards and Technology, an agency of the US government. Not subject to copyright in the USA. Trade names are provided only to specify procedures adequately and do not imply endorsement by the National Institute of Standards and Technology. Similar products by other manufacturers may be found to work as well or better.

References

1 F. Sanger, S. Nicklen and A.R. Coulson, DNA sequencing with chain-terminating inhibitors, *Proc. Natl. Acad. Sci. U. S. A.*, 1977, **74**(12), 5463–5467.
2 J. Shendure, *et al.*, Advanced sequencing technologies: methods and goals, *Nat. Rev. Genet.*, 2004, **5**(5), 335–344.
3 J. Shendure and H. Ji, Next-generation DNA sequencing, *Nat. Biotechnol.*, 2008, **26**(10), 1135–1145.
4 J.J. Kasianowicz, *et al.*, Characterization of individual polynucleotide molecules using a membrane channel, *Proc. Natl. Acad. Sci. U. S. A.*, 1996, **93**(24), 13770–13773.
5 C.C. Harrell, *et al.*, Resistive-Pulse DNA Detection with a Conical Nanopore Sensor, *Langmuir*, 2006, **22**(25), 10837–10843.
6 J. He, *et al.*, Identification of DNA Basepairing *via* Tunnel-Current Decay, *Nano Lett.*, 2007, **7**(12), 3854–3858.
7 S. Garaj, *et al.*, Graphene as a subnanometre trans-electrode membrane, *Nature*, 2010, **467**(7312), 190–193.
8 D.B. Wells, *et al.*, Assessing Graphene Nanopores for Sequencing DNA, *Nano Lett.*, 2012, **12**(8), 4117–4123.
9 G.F. Schneider, *et al.*, DNA Translocation through Graphene Nanopores, *Nano Lett.*, 2010, **10**(8), 3163–3167.
10 C.A. Merchant, *et al.*, DNA Translocation through Graphene Nanopores, *Nano Lett.*, 2010, **10**(8), 2915–2921.
11 S.K. Min, *et al.*, Fast DNA sequencing with a graphene-based nanochannel device, *Nat. Nanotechnol.*, 2011, **6**(3), 162–165.
12 N. Dontschuk, *et al.*, A graphene field-effect transistor as a molecule-specific probe of DNA nucleobases, *Nat. Commun.*, 2015, **6**, 6563.
13 T. Nelson, B. Zhang and O.V. Prezhdo, Detection of Nucleic Acids with Graphene Nanopores: Ab Initio Characterization of a Novel Sequencing Device, *Nano Lett.*, 2010, **10**(9), 3237–3242.
14 H.W.C. Postma, Rapid Sequencing of Individual DNA Molecules in Graphene Nanogaps, *Nano Lett.*, 2010, **10**(2), 420–425.
15 F. Traversi, *et al.*, Detecting the translocation of DNA through a nanopore using graphene nanoribbons, *Nat. Nanotechnol.*, 2013, **8**(12), 939–945.
16 C. Spencer and W. Meni, Challenges in DNA motion control and sequence readout using nanopore devices, *Nanotechnology*, 2015, **26**(7), 074004.
17 D. Branton, *et al.*, The potential and challenges of nanopore sequencing, *Nat. Biotechnol.*, 2008, **26**(10), 1146–1153.
18 M. Zwolak and M.D. Ventra, Colloquium: Physical approaches to DNA sequencing and detection, *Rev. Mod. Phys.*, 2008, **80**(1), 141–165.
19 V. Georgakilas, *et al.*, Functionalization of Graphene: Covalent and Non-Covalent Approaches, Derivatives and Applications, *Chem. Rev.*, 2012, **112**(11), 6156–6214.
20 J. Prasongkit, *et al.*, Theoretical Study of Electronic Transport through DNA Nucleotides in a Double-Functionalized Graphene Nanogap, *J. Phys. Chem. C*, 2013, **117**(29), 15421–15428.
21 M.J. Frisch, *et al.*, *Gaussian 09*, Gaussian, Inc., Wallingford, CT, USA, 2009.
22 A.D. Becke, Density-functional thermochemistry. III. The role of exact exchange, *J. Chem. Phys.*, 1993, **98**(7), 5648–5652.
23 C. Lee, W. Yang and R.G. Parr, Development of the Colle-Salvetti correlation-energy formula into a functional of the electron density, *Phys. Rev. B: Condens. Matter*, 1988, **37**(2), 785–789.

24 C.M. Breneman and K.B. Wiberg, Determining atom-centered monopoles from molecular electrostatic potentials. The need for high sampling density in formamide conformational analysis, *J. Comput. Chem.*, 1990, **11**(3), 361–373.
25 W.L. Jorgensen and J. Tirado-Rives, The OPLS [optimized potentials for liquid simulations] potential functions for proteins, energy minimizations for crystals of cyclic peptides and crambin, *J. Am. Chem. Soc.*, 1988, **110**(6), 1657–1666.
26 W.L. Jorgensen, D.S. Maxwell and J. Tirado-Rives, Development and Testing of the OPLS All-Atom Force Field on Conformational Energetics and Properties of Organic Liquids, *J. Am. Chem. Soc.*, 1996, **118**(45), 11225–11236.
27 L. Lindsay and D.A. Broido, Optimized Tersoff and Brenner empirical potential parameters for lattice dynamics and phonon thermal transport in carbon nanotubes and graphene, *Phys. Rev. B: Condens. Matter*, 2010, **81**(20), 205441.
28 A. Smolyanitsky, Molecular dynamics simulation of thermal ripples in graphene with bond-order-informed harmonic constraints, *Nanotechnology*, 2014, **25**(48), 485701.
29 H.W. Horn, *et al.*, Development of an improved four-site water model for biomolecular simulations: TIP4P-Ew, *J. Chem. Phys.*, 2004, **120**(20), 9665–9678.
30 J.L.F. Abascal, *et al.*, A potential model for the study of ices and amorphous water: TIP4P/Ice, *J. Chem. Phys.*, 2005, **122**(23), 234511.
31 D. Van Der Spoel, *et al.*, GROMACS: Fast, flexible, and free, *J. Comput. Chem.*, 2005, **26**(16), 1701–1718.
32 B. Hess, *et al.*, GROMACS 4: Algorithms for Highly Efficient, Load-Balanced, and Scalable Molecular Simulation, *J. Chem. Theor. Comput.*, 2008, **4**(3), 435–447.
33 K. Hatch, *et al.*, Demonstration that the shear force required to separate short double-stranded DNA does not increase significantly with sequence length for sequences longer than 25 base pairs, *Phys. Rev. E: Stat. Phys., Plasmas, Fluids, Relat. Interdiscip. Top.*, 2008, **78**(1), 011920.
34 T. Boland and B.D. Ratner, Direct measurement of hydrogen bonding in DNA nucleotide bases by atomic force microscopy, *Proc. Natl. Acad. Sci. U. S. A.*, 1995, **92**(12), 5297–5301.
35 E.D. Minot, *et al.*, Tuning Carbon Nanotube Band Gaps with Strain, *Phys. Rev. Lett.*, 2003, **90**(15), 156401.
36 A. Isacsson, Nanomechanical displacement detection using coherent transport in graphene nanoribbon resonators, *Phys. Rev. B: Condens. Matter*, 2011, **84**(12), 125452.
37 D.A. Cosma, *et al.*, Strain-induced modifications of transport in gated graphene nanoribbons, *Phys. Rev. B: Condens. Matter*, 2014, **90**(24), 245409.
38 S. Datta, *Electron Transport in Mesoscopic Systems*, Cambridge University Press, Cambridge, 1995.
39 E. Pop, V. Varshney and A.K. Roy, Thermal properties of graphene: Fundamentals and applications, *MRS Bull.*, 2012, **37**(12), 1273–1281.
40 A. Smolyanitsky and V.K. Tewary, Manipulation of graphene's dynamic ripples by local harmonic out-of-plane excitation, *Nanotechnology*, 2013, **24**(5), 055701.
41 Y. Feng, *et al.*, Nanopore-based Fourth-generation DNA Sequencing Technology, *Genomics, Proteomics Bioinf.*, 2015, **13**(1), 4–16.
42 G.F. Schneider, *et al.*, Tailoring the hydrophobicity of graphene for its use as nanopores for DNA translocation, *Nat. Commun.*, 2013, **4**, 2619.
43 J. Qi, *et al.*, Piezoelectric effect in chemical vapour deposition-grown atomic-monolayer triangular molybdenum disulfide piezotronics, *Nat. Commun.*, 2015, **6**, 7430.